Available online at www.sciencedirect.com
SCIENCE DIRECT®
Sensors and Actuators B 106 (2005) 758–765
SENSORS AND ACTUATORS B CHEMICAL
www.elsevier.com/locate/snb

Use of $La_{0.85}Sr_{0.15}CrO_3$ in high-temperature NO_x sensing elements

D.L. West*, F.C. Montgomery, T.R. Armstrong

Metals and Ceramics Division, Oak Ridge National Laboratory, Bldg 4508, MS 6083, Oak Ridge, TN 37831, USA

Received 17 March 2004; received in revised form 15 September 2004; accepted 23 September 2004

Abstract

This work focuses on use of the electronically-conducting oxide $La_{0.85}Sr_{0.15}CrO_3$ (LSC) in solid electrolyte-based NO_x sensing elements intended for operation at $T \sim 650\,^{\circ}C$. Two different investigations are described, in the first LSC was used as a direct substitute for Pt. The substitution led to decreased sensitivity to NO_2 and an enhancement of the NO response, although the NO_2 response was still much larger in magnitude and opposite in sign. Fabrication and evaluation of sensing elements with co-planar LSC and Pt electrodes comprised the second investigation. The measured NO_x sensing performance of these elements was commensurate with that of the elements fabricated in the first phase of the investigation (e.g., 450 ppm_v NO_2 in 7 vol% O_2 produced ~50 mV at 600 °C) and the response/recovery times for NO_2 sensing were improved. The results indicate that LSC could be useful in these types of sensing elements, both as a substitute for, and in combination with, Pt.

Keywords: Gas sensors; Lanthanum strontium chromite; Nitrogen dioxide; Nitrogen monoxide

1. Introduction

Oxides of nitrogen ("NO_x", a mixture of primarily NO and NO_2) are formed during combustion processes and are considered pollutants if exhausted to the atmosphere. These pollutants are typically removed from large-scale, fixed installations by selective catalytic reduction (SCR) and other technologies [1]. Currently, NO_x is removed from spark-ignited, passenger-car engine exhausts with a three-way catalyst (TWC), but the TWC is only effective for NO_x removal if the oxygen level in the exhaust is controlled within narrow limits [2]. Therefore, the current TWC cannot be applied to exhaust treatment for diesel engines and "lean-burn" gasoline engines, as the exhaust from these engines is too oxygen-rich for effective operation of the TWC.

If a TWC suitable for use in oxygen-rich exhausts is not developed, then some type of on-board remediation scheme must be employed to reduce the NO_x levels. Many of the on-board remediation techniques under investigation (such as SCR with urea) require the injection of species that themselves would be considered pollutants (or decompose into pollutants) if exhausted or "slipped" into the atmosphere. Thus, it is essential to develop compact and accurate sensors that can measure NO_x levels in oxygen-rich exhausts to aid in the precise dispensation of reducing agents. The ideal sensor would be operative at temperatures around 700 °C, capable of sensing NO_x levels in the range of 100–1000 ppm, and relatively insensitive to $[O_2]$ variations in the exhaust gas [3].

Two approaches to NO_x sensing at "high temperature" ($T \sim 700\,^{\circ}C$) using electroceramics have appeared in the literature: "amperometric" or "limiting-current" methods [4,5] and "mixed-potential" methods [6,7]. Amperometric techniques rely on measuring the oxygen-ion current generated by electrochemical decomposition of NO_x. The major challenge for this technique is separating the current due to the decomposition of NO_x from that due to the decomposition of O_2. One approach [8] which has been commercially applied, employs sequential chambers (reaction zones), the first zone for removal of O_2 and the second for electrochemical decomposition of NO_x (specifically, nitric oxide (NO)).

* Corresponding author. Tel.: +1 865 576 2264; fax: +1 865 574 4357.
E-mail address: westdl@ornl.gov (D.L. West).

0925-4005/$ – see front matter © 2004 Elsevier B.V. All rights reserved.
doi:10.1016/j.snb.2004.09.028

"Mixed-potential" sensing typically involves measuring the potential developed between two different electrodes. A mixed potential [9,10] arises when cathodic (reduction) and anodic (oxidation) reactions involving NO_x and O_2 occur simultaneously on an electrode. Each of the reactions has a defined *V–I* characteristic. If the net current ($I_{cathodic} + I_{anodic}$) across the electrode is held at zero, then there will be a unique voltage at which $|I_{cathodic}| = |I_{anodic}|$ for a given [NO_x] and [O_2]. The mixed potential is an example of a "non-Nernstian" or "non-equilibrium" phenomenon [5], wherein the potential developed between two electrodes on an oxygen-ion conducting electrolyte is not governed strictly by the partial pressure of O_2 over each electrode.

The present investigation explores the application of the electronically-conducting oxide $La_{0.85}Sr_{0.15}CrO_3$ (LSC) [11,12] in non-Nernstian NO_x sensing elements. First, LSC was employed as a direct substitute for Pt. Pt is costly and can be catalytic for oxidation and other electrochemical phenomena. Therefore, such a substitution could lower the materials cost of the elements, afford more opportunity to engineer the element microstructure, and allow (through composition modification of the electronically-conducting oxide) one to tailor the electrochemical and catalytic behavior of the elements. The general approach for this phase of the investigation was to fabricate sensing elements differing only in the material used as the electronic conductor (LSC or Pt).

For the second phase of the investigation, sensing elements with co-planar LSC and Pt electrodes were fabricated. This material combination has been used previously for potentiometric NO_x sensing devices [13], but the present investigation differs in that a co-planar design without an air reference was employed.

2. Experimental procedure

Fig. 1 shows the multi-layered sensing element geometry for the first phase of the investigation (substitution of LSC for Pt). The substrate for the sensing elements was yttria-stabilized zirconia (YSZ) (8 mol% Y_2O_3–substituted ZrO_2, TZ–8Y, Tosoh, NJ). The YSZ was tape cast, laminated, and sintered at 1350 °C for 2 h in air to produce disk-shaped forms about 1.6 cm in diameter and 0.1 cm in thickness.

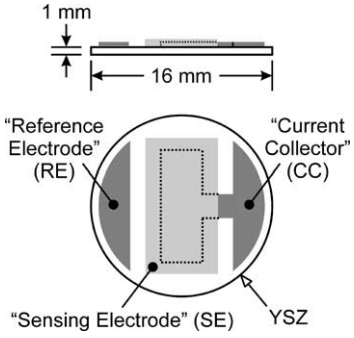

Fig. 1. Sensing element geometry for investigating the substitution of LSC for Pt. The element consists of two screen-printed layers on a yttria-stabilized zirconia (YSZ) substrate.

Table 1
Specimens prepared to investigate the substitution of $La_{0.85}Sr_{0.15}CrO_3$ (LSC) for Pt

Sample ID	SE material	RE/CC material
NC2/Pt	$NiCr_2O_4$[a]	Pt[b]
NC2/LSC	$NiCr_2O_4$	$La_{0.85}Sr_{0.15}CrO_3$[c]
LSCF/Pt	$La_{0.6}Sr_{0.4}Co_{0.2}Fe_{0.8}O_3$[d]	Pt
LSCF/LSC	$La_{0.6}Sr_{0.4}Co_{0.2}Fe_{0.8}O_3$	$La_{0.85}Sr_{0.15}CrO_3$

The RE/CC and SE are defined in Fig. 1. For all electrode materials other than Pt, screen-printing inks were fabricated in-house from the listed oxides.
[a] Cerac (Milwaukee, WI) #N-1086.
[b] Electroscience (King of Prussia, PA) #5547-1F-P.
[c] Praxair Specialty Ceramics (Woodinville, WA) #03-P3286.
[d] Praxair #03-P4065.

A patterned layer of either LSC or Pt, comprising the reference electrode (RE) and current collector (CC) (Fig. 1), was screen-printed onto one broad face of the YSZ disks, air-dried, and fired at 1100 °C for 0.3 h in air. A second screen-printed layer, the sensing electrode (SE), was then patterned over a portion of the CC as shown in Fig. 1, air-dried, and fired at 1100 °C for 1 h in air.

The effect of substituting an electronically-conducting oxide (LSC) for Pt was studied by fabricating two pairs of sensing elements with nominally identical SE materials. The elements prepared are listed in Table 1 and consisted of $NiCr_2O_4$ (NC2) SE layers and $La_{0.8}Sr_{0.2}Co_{0.4}Fe_{0.6}O_3$ (LSCF) SE layers on both Pt and LSC RE/CC's.

Element geometries for the second phase of the investigation are shown in Fig. 2. These LSC|YSZ|Pt elements also were based on a YSZ substrate and consisted of co-planar LSC and Pt electrodes prepared by screen printing and thermal treatment as described above. One element geometry consisted of semicircular electrodes on opposite halves of one face of the YSZ substrate while the other consisted of interdigitated LSC and Pt electrodes.

The response of the prototype devices was measured with the apparatus shown in Fig. 3. A four-inlet gas-mixing unit (Environics (Tolland, CT) 4000) was used to mix N_2, O_2, and NO_x (either NO (7000 ppm_v in N_2) or NO_2 (5000 ppm_v in N_2)) at room temperature. The composition of the test gas mixtures was typically in the range 7 vol% ≤ [O_2] ≤ 20 vol%, 300 ppm_v ≤ [NO_x] ≤ 1500 ppm_v, with the balance being N_2.

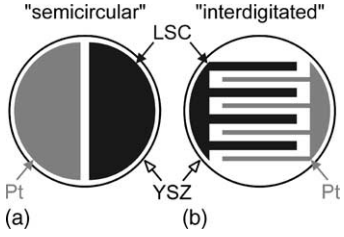

Fig. 2. Sensing elements with co-planar LSC and Pt electrodes. The diameter and thickness of the YSZ substrate are identical to the element shown in Fig. 1.

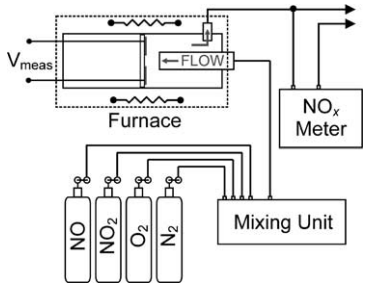

Fig. 3. Schematic setup of apparatus for gas handling, sensor response measurement, and NO_x monitoring.

(These concentrations were felt to be representative of fairly NO_x-rich exhausts, as might be encountered with a lean-burn gasoline engine [3].) The gas mixtures were presented (at a flow rate of 750 sccm) to the electroded side of the sensing elements. Local heating of the sensor was not employed, rather as shown in Fig. 3 the sensor was centrally located in a ~2.5 cm diameter Al_2O_3 tube placed horizontally in a resistively-heated furnace.

The voltage developed between the SE/CC and RE (for the element geometry shown in Fig. 1), or between the LSC and Pt (for the element geometries shown in Fig. 2) was measured with a Keithley (Cleveland, OH) 617 electrometer and a chemiluminescent NO_x meter (TEI, Franklin, MA, 42CHL) was used to independently measure the NO_x levels in the gas mixtures exiting the furnace. The sample temperature was monitored using a type K thermocouple placed ~0.5 cm from the electroded surface of the specimen, and was typically found to be within ± 5 °C of the furnace temperature.

Most testing in the present investigation was conducted in an isothermal manner, with the specimen being subjected to either sequential changes in input [NO_x] at a fixed O_2 concentration (7 vol%) or sequential changes in O_2 concentration at a fixed input [NO_x] (450 or 1500 ppm_v). Some sample response traces are shown in Fig. 4. In all cases, for the tests conducted as shown in Fig. 4, the average of the voltage readings over the last minute at each test gas condition was taken as "V_{meas}" for that condition. The "sensing response" (ΔV) as a function of input [NO_x] and [O_2] was then determined by subtracting "V_{meas}" at a given input [NO_x] and [O_2] from the (typically small, see Fig. 4) measured voltage "V_o" at 0 ppm_v input NO_x and 7 vol% O_2:

$$\Delta V\,(X[\mathrm{NO}_x],\,7\ \mathrm{vol\%\,O_2}) \equiv V_{\mathrm{meas}}^{X[\mathrm{NO}_x],\,7\ \mathrm{vol\%\,O_2}} - V_{\mathrm{o}},$$

$$\Delta V\,(\mathrm{input}[\mathrm{NO}_x],\,Y\ \mathrm{vol\%\,O_2}) \equiv V_{\mathrm{meas}}^{\mathrm{input}[\mathrm{NO}_x],\,Y\ \mathrm{vol\%\,O_2}} - V_{\mathrm{o}},$$

$$V_{\mathrm{o}} = V_{\mathrm{meas}}^{0\ \mathrm{ppm_v NO}_x,\,7\ \mathrm{vol\%\,O_2}} \quad (1)$$

Electrode microstructures were characterized by examining screen-printed and fired electrode surfaces (post-test) with a Hitachi S-800 SEM operating at 5 kV accelerating voltage. The samples were coated with C in an evaporator before examination in the SEM.

3. Results and discussion

3.1. Electrode microstructures

Fig. 5 shows electrode microstructures (post-test, from elements with the geometry shown in Fig. 1) in plan view. In all cases, the screen-printing and subsequent thermal treatment had produced porous layers of the electrode materials, which are desirable for the intended gas-sensing application. The Pt RE (Fig. 5a) features somewhat of a bi-modal particle size distribution with larger fissures or cracks while the LSC RE (Fig. 5b) is a weakly sintered assemblage of nearly uniform-sized particles. The LSCF and $NiCr_2O_4$ SE's (Fig. 5c and d) are comprised of sintered agglomerates, with the $NiCr_2O_4$ particles exhibiting distinct facets. Cross-sectioning, polishing, and examination with optical microscopy of samples pre-

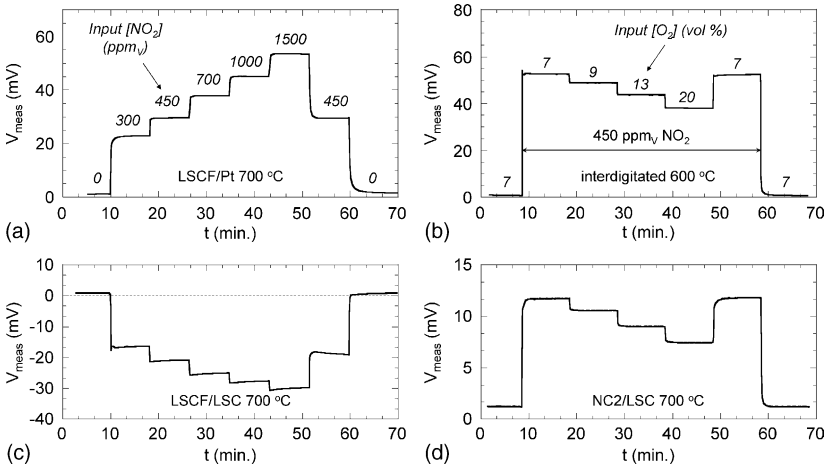

Fig. 4. Sample response traces. The response of the LSCF/Pt and LSCF/LSC samples to variations in input [NO_2] at fixed [O_2] (7 vol%) are shown in (a) and (c) while the response of the interdigitated and NC2/LSC samples to variations in input [O_2] at fixed [NO_2] (450 ppm_v) are shown in (b) and (d). The [NO_2] variations for (a) and (c), and the [O_2] variations for (b) and (d) were nominally identical.

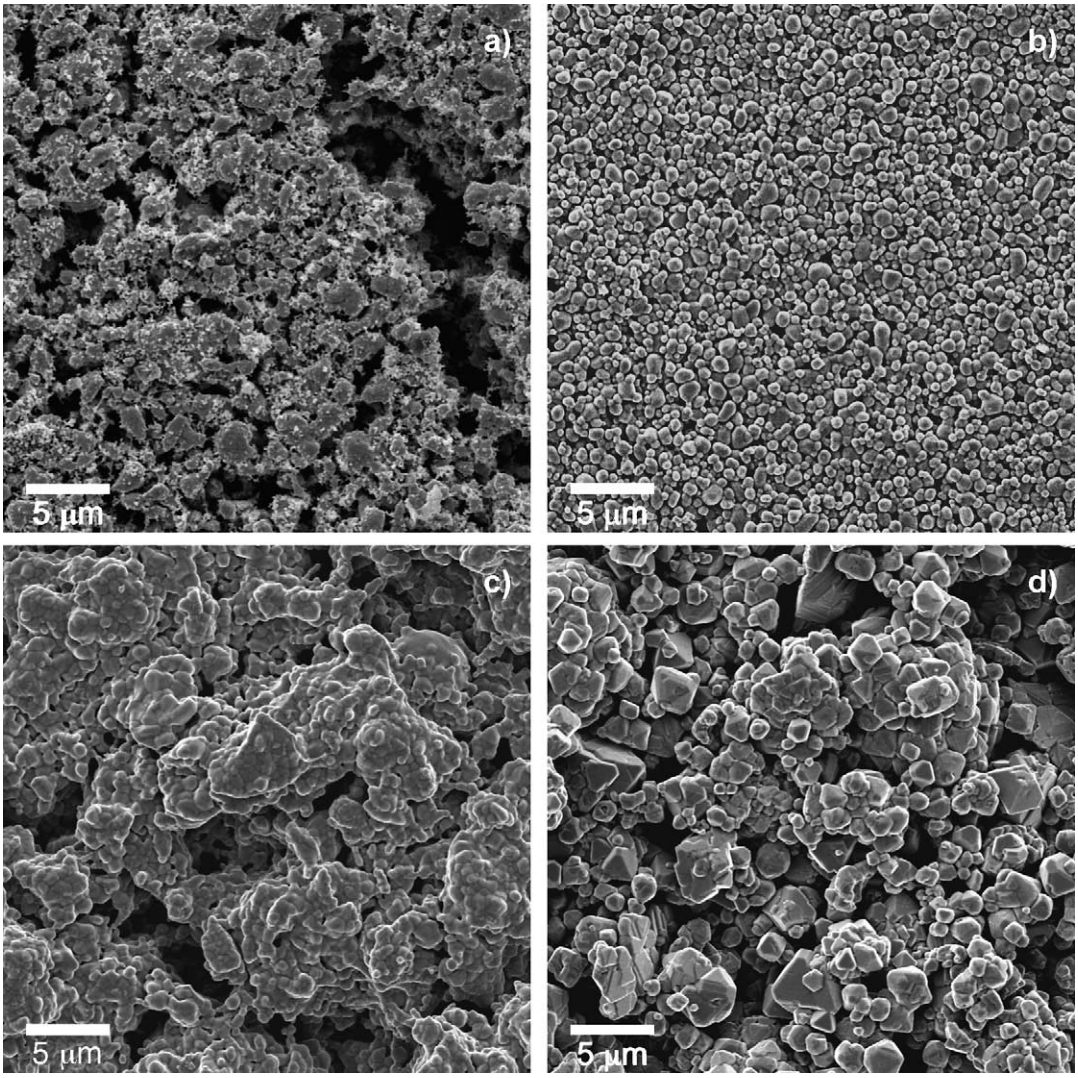

Fig. 5. Electrode microstructures: (a) Pt, (b) $La_{0.85}Sr_{0.15}CrO_3$ (LSC), (c) $La_{0.8}Sr_{0.2}Co_{0.2}Fe_{0.8}O_3$ (LSCF), and (d) $NiCr_2O_4$ (NC2). Secondary electron images at 5 kV (Hitachi S-800).

pared in similar fashion to those in Fig. 5 indicated that the dried and fired thickness of the electrode layers was typically ~20 μm.

3.2. Substitution of LSC for Pt-sensing performance

The sensing responses (calculated using Eq. (1)) to NO_2 at 7 vol% O_2 for the samples listed in Table 1 are shown in Fig. 6a. The response of the samples to changes in input [NO_2] were fit to a logarithmic expression:

$$\Delta V\,(\mathrm{mV}) = m \log_{10}[\text{input NO}_2\,(\text{ppm}_\text{v})] + \text{b}, \quad (2)$$

and the resulting correlation coefficients (R^2) were all ≥0.92. This indicates that the response of both the LSC and Pt-containing samples to NO_2 (at 7 vol% O_2) was in accord with a model posited by Miura for mixed-potential sensing of several reducing gas species (e.g., CO [14], H_2S [15], and H_2 [16]). Miura's model, which assumes a Butler–Volmer type [17] relation between current density (j) and potential (V), and a power-law dependence of j on concentration, predicts for the measured voltage as a function of concentration:

$$V_{\text{meas}} = C_1 + C_2 \ln[\text{Re}]\,(\text{fixed}\,[O_2]),$$
$$V_{\text{meas}} = C_3 + C_4 \ln[O_2]\,(\text{fixed}\,[\text{Re}]), \quad (3)$$

where C_1, C_2, C_3, and C_4 are constants and Re indicates a reducing gas.

It is apparent from Fig. 6a that the substitution of LSC for Pt has not systematically affected the magnitude of the NO_2 responses. However, the sensing elements with LSC as the RE/CC material consistently displayed less sensitivity to NO_2 (i.e., the slope m resulting from the fit of ΔV versus log[NO_2] was smaller, and the voltage change induced by 300 ppm_v NO_2 was nearly equal to that induced by 1500 ppm_v NO_2). This indicates that sensing elements with LSC as the RE/CC might be best suited for detection of very low levels of NO_2.

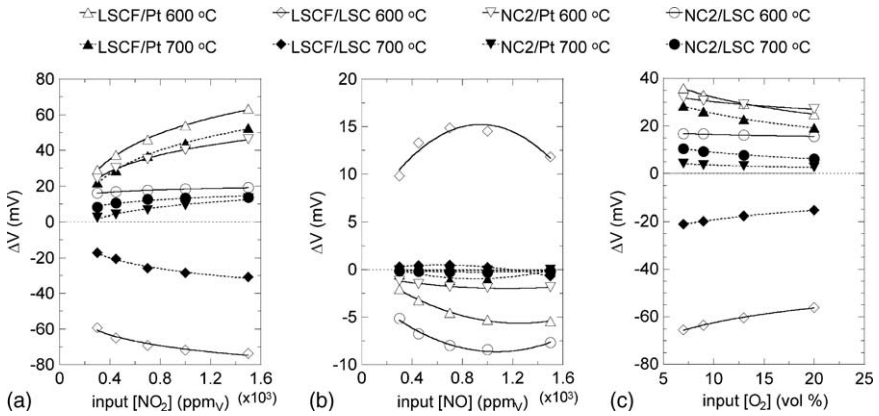

Fig. 6. Sensing performance of the multi-layered elements in Table 1. The response to input NO_2 and NO (both at 7 vol% O_2) are shown in (a) and (b), respectively while (c) shows the $[O_2]$ dependence of the response to 450 ppm_v NO_2. The lines drawn in (a) and (c) correspond to logarithmic fits and those drawn in (b) correspond to (second-order) polynomial fits.

The response of the multi-layered samples to input NO (Fig. 6b) was opposite in sign to, and more difficult to interpret, than the response to input NO_2. Using only NO in the test gas mixtures, virtually no response was observed at 700 °C, irrespective of the RE/CC material (LSC or Pt). However, the response of the LSC-containing samples to input NO was much stronger than that of the Pt-containing samples at 600 °C.

In general, the small magnitude of the sensing responses in Fig. 6b, combined with their tendency to either plateau or inflect at larger [NO], indicate that these sensing elements are not well-suited for the sensing of NO at temperatures near 600 °C. Use of these sensing elements for $[NO_x]$ determination at this temperature would seemingly require either equilibration of the NO/NO_2 ratio at a temperature lower than the sensing element temperature (as described by Szabo and Dutta [18]) or electrochemical conversion to NO_2 (as described by Kunimoto et al. [19]). Since in either of these sensor designs the NO_2 response is most important, further characterization of sensing element response focused on NO_2.

Eq. (3) predicts that the response of these sensing elements is a logarithmic function of $[O_2]$ at fixed $[NO_2]$. Fig. 6c shows the measured $[O_2]$ dependence of the sensor response at an input $[NO_2]$ of 450 ppm_v. (The nature of the O_2 dependence was similar for higher input $[NO_2]$ (1500 ppm_v).) The logarithmic dependence predicted by Eq. (3) was observed for both the LSC- and Pt-containing samples. The regressions on (ΔV) versus $\log[O_2]$ produced correlation coefficients ≥ 0.98 in all instances. In contrast to the NO_2 sensitivity discussed above, there was not a systematic trend in the effect of LSC substitution on the $[O_2]$ dependence of the NO_2 response.

A pronounced response/recovery asymmetry (to introduction/removal of 450 ppm_v NO_2 (in 7 vol% O_2)) was observed for the sensing elements of Table 1. This is illustrated in Fig. 7, which shows the response of the sensing elements to the introduction of 450 ppm_v NO_2 (Fig. 7a) and the removal of 450 ppm_v NO_2 (Fig. 7b). For the introduction of NO_2, the 90% response time of all the elements at 600 and 700 °C is about 5 s, which is the temporal resolution of the experiment. The recovery upon removal of NO_2 is much less rapid, particularly for the LSC-containing samples at 600 °C.

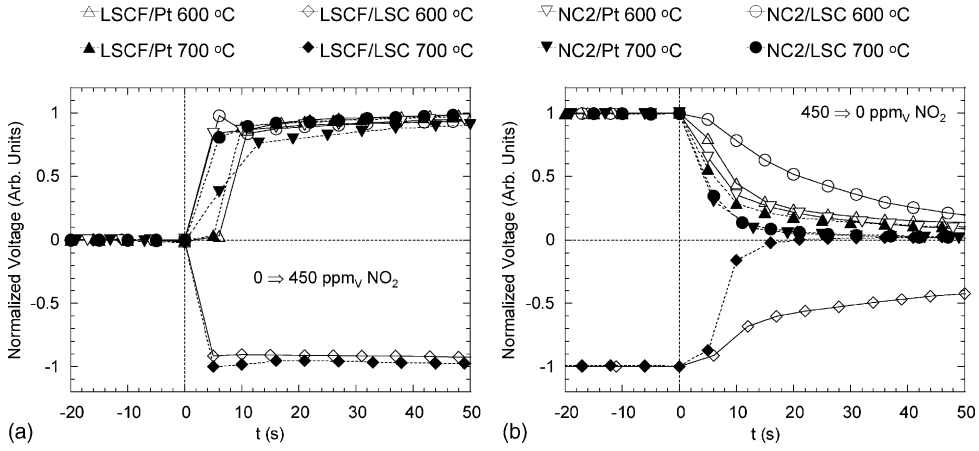

Fig. 7. Response of the samples in Table 1 to the introduction of 450 ppm_v NO_2 (a) and the removal of 450 ppm_v NO_2 (b). Data collected in 7 vol% O_2. Lines are drawn as an aid to the eye.

Lundström [20] has discussed the adsorption and desorption processes that might govern the response and recovery rates of solid-state gas sensors operating at ~500 °C. Although the sensing mechanism of the solid-state sensors described in [20] is thought to be quite different than that of the sensing elements investigated here, similar considerations may govern the response/recovery kinetics. As mentioned previously, the NO_2 step response times of the multi-layered sensing elements (Fig. 7a) was on the order of the experimental resolution and thus could not be analyzed further, but the more sluggish step recoveries (Fig. 7b) were fit to the expressions proposed in [20]:

$$V = V_s \exp(-t/\tau_r) \text{ (first-order desorption)}, \quad (4a)$$

$$V = V_s/(1 + 2V_s t/\tau_r) \text{ (second-order desorption)}, \quad (4b)$$

where V_s is the steady-state sensor response and τ_r is the inverse of the desorption rate. For the sensing elements in Fig. 7b), it was found that the recovery from NO_2 exposure was typically better described by Eq. (4b) than Eq. (4a), with both fits yielding nearly identical values of τ_r (~50 and ~15 s for the LSC- and Pt-containing samples, respectively at 600 °C and ~5 s for all the sensing elements at 700 °C).

Fig. 6a and b shows that at 600 °C the substitution of LSC for Pt as the RE/CC material changed the sign of the NO_x response for the LSCF samples, but not that of the NC2 samples:

$$\Delta V_{NO_2}^{LSCF/Pt}, \Delta V_{NO}^{LSCF/LSC}, \Delta V_{NO_2}^{NC2/Pt}, \Delta V_{NO_2}^{NC2/LSC} > 0, \text{ and}$$
$$\Delta V_{NO}^{LSCF/Pt}, \Delta V_{NO_2}^{LSCF/LSC}, \Delta V_{NO}^{NC2/Pt}, \Delta V_{NO}^{NC2/LSC} < 0 \quad (5)$$

Further, LSCF/Pt produced the largest positive signals in NO_2 and LSCF/LSC produced the largest negative signals in NO_2 (Fig. 6a). This pointed to different electrochemical behaviors of LSC and Pt in the NO_x and O_2 containing gas mixtures and prompted the investigation of sensing elements with the construction LSC|YSZ|Pt as shown in Fig. 2. These investigations are described in the immediately following section.

3.3. LSC|YSZ|Pt-sensing elements—sensing performance

Fig. 8 shows the measured NO_x sensing performance of the LSC|YSZ|Pt-sensing elements (Fig. 2). As was the case with the multi-layered elements (Fig. 6), the response to NO_2 (Fig. 8a) was much stronger than that to NO (Fig. 8b), and the two different NO_x species produced signals that were opposite in sign. The semicircular geometry yielded both higher signals and higher sensitivity to NO_2, but the $[O_2]$ dependence of the NO_2 response was similar for both geometries (Fig. 8a and c). Since only a single element of each geometry (semicircular and interdigitated) was fabricated and tested, it is not clear whether the larger NO_2 response and sensitivity of the semicircular geometry reflect electrode geometry factors or simply element-to-element variability.

The NO_2 response (in 7 vol% O_2) (Fig. 8a) and the $[O_2]$ dependence of the 450 ppm_v NO_2 response (Fig. 8c) for both electrode geometries in Fig. 2 were well described by logarithmic functions in most instances, but deviations from this behavior were observed for the NO_2 response of both geometries at 700 °C. At this temperature the measured NO_2 responses for both geometries were nearly linear, with a second-order polynomial providing the best fit. Garzon et al. [7] reported linear responses for a mixed-potential CO sensing element (with the construction $Pt|Ce_{0.8}Gd_{0.2}O_{1.9}|Au$) operating at 600 °C and attributed the linear behavior to diffusion-limited behavior of the anodic reaction ($CO \Rightarrow CO_2$) and Ohmic (low overpotential) behavior of the cathodic reaction (O_2 (g) $\Rightarrow O^{2-}$). Whether similar considerations apply to the behavior observed here at 700 °C remains to be determined.

The step response/recovery asymmetry (with 450 ppm_v NO_2 in 7 vol% O_2) described previously was also observed with both the semicircular and interdigitated geometries. Representative data are shown in Fig. 9, which illustrates

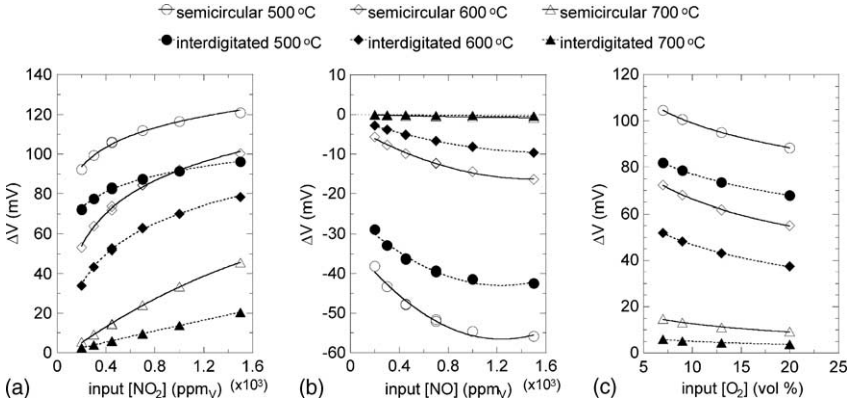

Fig. 8. Sensing response of the elements shown schematically in Fig. 2. The responses to input NO_2 and NO (both in 7 vol% O_2) are shown in (a) and (b), while (c) shows the $[O_2]$ dependence of the response to 450 ppm_v NO_2. The lines drawn in (a) (except for the data at 700 °C) and (c) are logarithmic fits, all other lines drawn correspond to second-order polynomial fits.

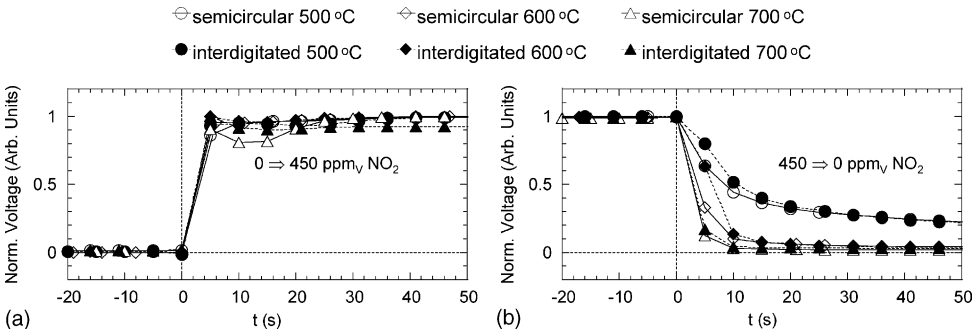

Fig. 9. Response of the samples in Fig. 2 to introduction of 450 ppm_v NO_2 (a), and removal of 450 ppm_v NO_2 (b), both in 7 vol% O_2. Lines are drawn as an aid to the eye.

that the response time is temperature and geometry independent (within the resolution of the experiment (∼5 s)) over the temperature range 500–700 °C, while the recovery time is independent of geometry but dependent on temperature.

In general, the recovery of the sensing elements in Fig. 9 from exposure to NO_2 was better described by Eq. (4b) than Eq. (4a), and the values of τ_r obtained from the fits (∼30, ∼5, and ∼1 s for 500, 600, and 700 °C, respectively) indicated that the recovery of these elements was faster than that of the multi-layered element geometry shown in Fig. 1. This is also evident from a visual comparison of Figs. 7b and 9b.

4. Conclusions

Direct substitution of LSC for Pt has been investigated with multi-layered sensing elements of the geometry shown in Fig. 1. Systematically, the substitution of LSC for Pt appeared to lower the NO_2 sensitivity, increase the magnitude of the NO response and lead to long recovery times (from exposure to NO_2) at 600 °C. Sensing elements with co-planar LSC–Pt electrodes (Fig. 2) could be suitable as NO_2 sensing elements at 600–700 °C, and appear to offer improved response/recovery times compared to the multi-layered geometry.

Acknowledgements

The authors wish to thank C.A. Walls for fabricating the YSZ substrates, B.L. Armstrong for formulating and producing the screen-printing inks, S.B. Waters for assistance with electron microscopy, and D. Kubinski and R. Soltis of Ford Scientific Research Laboratories (Dearborn, MI) for consultation in automotive sensing requirements. Oak Ridge National Laboratory is operated by UT-Battelle, LLC for the U.S. Department of Energy under contract DE-AC05-00OR22725.

References

[1] K.B.J. Schnelle, C.A. Brown, NO_x control, in: Air Pollution Control Technology Handbook, CRC Press, Boca Raton, 2001, pp. 241–255.
[2] J.T. Woestman, E.M. Logothetis, Controlling automotive emissions, Ind. Phys. 1 (1995) 21–24.
[3] F. Menil, V. Coillard, C. Lucat, Critical review of nitrogen monoxide sensors for exhaust gases of lean burn gasoline engines, Sens. Actuators B: Chem. 67 (2000) 1–23.
[4] N. Docquier, S. Candel, Combustion control and sensors: a review, Prog. Energy Combust. Sci. 28 (2002) 107–150.
[5] W. Gopel, R. Gotz, M. Rosch, Trends in the development of solid state amperometric and potentiometric high temperature sensors, Solid State Ionics 136–137 (2000) 519–531.
[6] N. Miura, G. Lu, N. Yamazoe, Progress in mixed-potential type devices based on solid electrolyte for sensing redox gases, Solid State Ionics 136–137 (2000) 533–542.
[7] F.H. Garzon, R. Mukundan, E.L. Brosha, Solid-state mixed potential gas sensors: theory, experiments, and challenges, Solid State Ionics 136–137 (2000) 633–638.
[8] N. Kato, H. Kurachi, Y. Hamada, Thick film ZrO_2 sensor for the measurement of low NO_x concentration, SAE Technical Paper 980170, 1998.
[9] N. Miura, H. Kurosawa, M. Hasei, G. Lu, N. Yamazoe, Stabilized zirconia-based sensor using oxide electrode for detection of NO_x in high-temperature combustion-exhausts, Solid State Ionics 86–88 (1996) 1069–1073.
[10] M.N. Mahmood, N. Bonanos, Application of the mixed potential model to the oxidation of methane on silver and nickel–zirconia catalysts, Solid State Ionics 53–56 (1992) 142–148.
[11] A.J. Moulson, J.M. Herbert, Electroceramics, Chapman and Hall, London, 1990, pp. 122–123.
[12] I. Yasuda, M. Hishinuma, Electrical conductivity and chemical diffusion coefficient of Sr-doped lanthanum chromites, Solid State Ionics 40 (1995) 141–150.
[13] V. Bruser, U. Lawrenz, S. Jakobs, H.-H. Mobius, U. Schonauer, NO_x-determination with galvanic zirconia solid electrolyte cells, Diffus. Defect Data B: Solid State Phenom. 39–40 (1994) 269–272.
[14] N. Miura, T. Raisen, G. Lu, N. Yamazoe, Highly selective CO sensor using stabilized zirconia and a couple of oxide electrodes, Sens. Actuators B: Chem. 47 (1998) 84–91.
[15] N. Miura, Y. Yan, G. Lu, N. Yamazoe, Sensing characteristics and mechanism of hydrogen sulfide sensor using stabilized zirconia and oxide sensing electrode, Sens. Actuators B: Chem. 34 (1996) 367–372.
[16] G. Lu, N. Miura, N. Yamazoe, High-temperature hydrogen sensor based on stabilized zirconia and a metal oxide electrode, Sens. Actuators B: Chem. 35–36 (1996) 130–135.

[17] P.W. Atkins, Physical Chemistry, fourth ed., W.H. Freeman, New York, 1989, pp. 906–917.
[18] N.F. Szabo, P.F. Dutta, Strategies for total NO_x measurement with minimal CO interference utilizing a microporous zeolitic catalytic filter, Sens. Actuators B: Chem. 88 (2002) 168–177.
[19] A. Kunimoto, M. Hasei, Y. Yan, Y. Gao, T. Ono, Y. Nakanouchi, New total-NO_x sensor based on mixed potential for automobiles, SAE Technical Paper 1999-01-1280, 1999.
[20] I. Lundström, Approaches and mechanisms to solid state based sensing, Sens. Actuators B: Chem. 35–36 (1996) 11–19.

Biographies

Dave West is a post-doctoral research associate at Oak Ridge National Laboratory (ORNL). He received a BA in Physics from the University of California in 1987 and MS and PhD degrees, both in Materials Science and Engineering, from the University of Washington (MS, 1996) and the University of Illinois (PhD, 2002).

Fred Montgomery is a senior staff scientist at ORNL, and holds BS and PhD degrees in Chemistry from the University of Oregon (BS, 1966) and the University of Rochester (PhD, 1971).

Tim Armstrong is the ORNL Hydrogen, Fuel Cell, and Infrastructure Manager. He received a BS in Ceramic Engineering from the Ohio State University (1984) and a PhD, also in Ceramic Engineering, from the University of Illinois (1989).